Evolution of the Southern Segment of the Philippine Trench: Constraints From Seismic Tomography

doi: 10.1029/2018GC007685

Geochemistry, Geophysics, Geosystems

RESEARCH ARTICLE
10.1029/2018GC007685

Key Points:
- Three subducting slabs are detected clearly in the upper mantle under the study region
- The Philippine Sea Plate subduction along the southern Philippine Trench initiated at 20-25 Ma
- The Molucca Sea closure resulted in subduction reorganization along the southern Philippine Trench at ~5 Ma

Supporting Information:
- Supporting Information S1

Correspondence to:
J. Fan,
fanjianke@qdio.ac.cn

Citation:
Fan, J., & Zhao, D. (2018). Evolution of the southern segment of the Philippine Trench: Constraints from seismic tomography. *Geochemistry, Geophysics, Geosystems*, *19*, 4612–4627. https://doi.org/10.1029/2018GC007685

Received 14 MAY 2018
Accepted 1 NOV 2018
Accepted article online 6 NOV 2018
Published online 27 NOV 2018

Evolution of the Southern Segment of the Philippine Trench: Constraints From Seismic Tomography

Jianke Fan[1,2] and Dapeng Zhao[3]

[1]CAS Key Laboratory of Marine Geology and Environment, Institute of Oceanology, Chinese Academy of Sciences, Qingdao, China, [2]Laboratory for Marine Geology, Qingdao National Laboratory for Marine Science and Technology, Qingdao, China, [3]Department of Geophysics, Tohoku University, Sendai, Japan

Abstract A high-resolution model of three-dimensional *P* wave tomography of the crust and upper mantle beneath the southern part of the Philippine Trench is determined by inverting 22,960 arrival times of 2,789 local earthquakes and 4,660 traveltime residuals of 751 teleseismic events simultaneously. The tomographic method TOMOG3D is used to obtain the tomographic model that has a lateral resolution of 0.6° or better, as shown by extensive checkerboard resolution tests. A model-recovery synthetic test is also performed, which indicates that main features of our tomographic images are quite robust. Our results show that the Philippine Sea slab has subducted down to depths of 450–600 km with an *overturned* dip angle along the southern segment of the Philippine Trench, indicating that the subduction of the Philippine Sea Plate along the southern segment of the Philippine Trench initiated at 20–25 Ma, contemporaneous with the Sangihe Trench. The subduction initiation of the Philippine Sea Plate at the central Philippine Trench resulted from the collision between the Philippines and the Palawan block at ~10 Ma. The subduction completion of the Molucca Sea slab propagated from the south to the north at ~5 Ma, which presumably resulted in the subduction reorganization of the Philippine Sea Plate along the southern segment of the Philippine Trench and subduction initiation of the Philippine Sea Plate along the northern segment of the Philippine Trench.

1. Introduction

The Philippine Trench (PT) fringes the southwestern margin of the Philippine Sea Plate (PSP) on the eastern side of the Philippine Archipelago, where the Eurasian, the Philippine Sea, and the Australian plates are interacting with each other (Figure 1). The PSP is subducting beneath the Philippine Archipelago along the PT, and the Celebes oceanic lithosphere is subducting beneath the Mindanao and Sulawesi islands along the Cotabato and Sulawesi trenches, respectively, whereas the Molucca Sea Plate has subducted beneath the Sulawesi-Sangihe and Halmahera islands along the Sangihe and Halmahera trenches, respectively, and the Sangihe and Halmahera arcs are colliding (Figure 1). The tectonics in this region is rendered particularly complex by the interplays between these subduction zones, among which the PT is accommodating more than 55% of the convergence between the PSP and the Eurasian Plate (Rangin et al., 1999). Therefore, the PT is a key component to understand the complicated tectonics in and around this region.

To date, the PT origin and evolution have been controversial. It is commonly considered that the PT originated from the flip of subduction along the Manila Trench from the west to the east (e.g., Cardwell et al., 1980), caused by the collision between some microcontinental blocks and the Philippine Archipelago at 8–9 Ma (Marchadier & Rangin, 1990). Mainly based on the spatial distribution of earthquakes and focal mechanism solutions, Cardwell et al. (1980) inferred that the PT southern part (2–6°N) is younger than its northern part (12–16°N), which was also suggested by Ozawa et al. (2004) showing that the oldest volcanism occurred at 6.6 Ma in the middle Philippines associated with the subduction along the PT, and the subduction was initiated from the north at 8–9 Ma and propagated to the south. However, they did not consider the northward movement of the Philippines during the last 30 Ma (Hall, 2002). Pubellier et al. (1996) suggested that the PT and the Philippine Fault (PF) coupled together and propagated from the north to the south, which is also supported by Aurelio (2000) who pointed out that the PT-PF system formed under a shear partitioning mechanism accompanied with the transformation of the relative movement of the PSP with respect to the Eurasian Plate from a northward to a northwestward motion. Lallemand et al. (1998) proposed that the collision between the Halmahera Arc and the Mindanao Island at 4–5 Ma gave rise to the subduction initiation of the PT central segment (6–12°N), and then the subduction propagated toward both the north and the

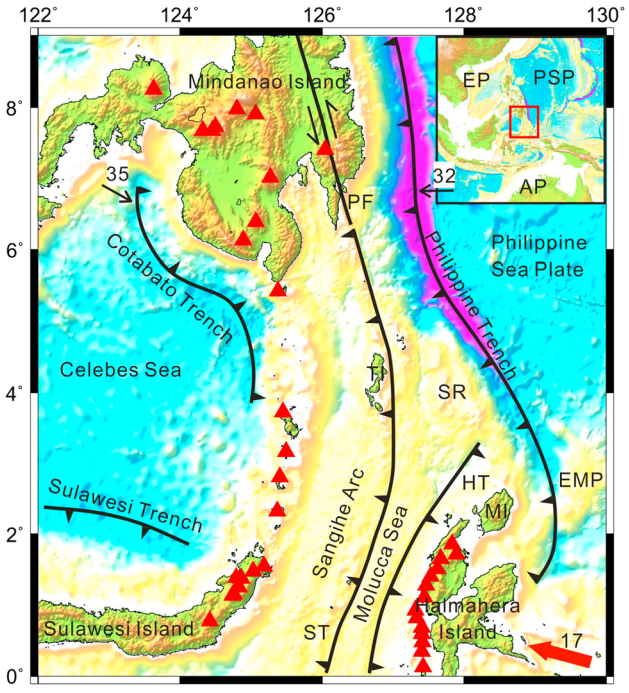

Figure 1. Tectonic background in and around the southern segment of the Philippine Trench. The bathymetric data are from Smith and Sandwell (1997). The saw-toothed lines denote trench axes, and the solid line shows the active Philippine fault (PF). The black arrows and adjacent numbers indicate the convergence rates (mm/year) along the Philippine Trench and the Cotabato Trench, and the red arrow and adjacent number indicate the relative rate near the boundary between the Philippine Sea Plate and the Australian Plate (Rangin et al., 1999). The red triangles denote active volcanoes from the Smithsonian Institution's Global Volcanism Program (2013). AP = the Australian Plate; EMP = the East Morotai Plateau; EP = the Eurasian Plate; HT = the Halmahera Trench; MI = the Morotai Island; PSP = the Philippine Sea Plate; SR = the Snellius Ridge; TI = the Talaud Island. The red box in the inset map shows the location of the present study region.

south. This proposal has been supported by results of seismic tomography (Fan et al., 2017), which show that the subducted depth of the Philippine Sea slab is greater under the middle PT than that under the northern PT. However, the depth of the Philippine Sea slab beneath the southern PT was not determined by Fan et al. (2017). Therefore, our understanding of the PT origin and evolution is very limited due to the scarcity of the morphologic information of the subducted Philippine Sea slab beneath the PT southern segment.

In this work, we determine a high-resolution model of *P* wave velocity (V_p) tomography of the crust and upper mantle beneath the southern PT, which sheds new light on the deep structure and tectonic evolution of the study region.

2. Data and Method

We used a large number of *P* wave arrival time data for tomographic inversions, which were selected from the International Seismological Center (ISC)-EHB Bulletins from 1960 to 2013 (http://www.isc.ac.uk/isc-ehb/). The ISC-EHB bulletin is a groomed version of the ISC bulletin, which contain teleseismically well-constrained events that are selected and relocated using the EHB algorithm (Engdahl, 2006; Engdahl et al., 1998) to minimize uncertainties in the hypocentral parameters. In particular, uncertainties of the focal depths are generally $<$15 km, thanks to the use of arrival times of depth phases (*pP*, *pwP*, and *sP*; Engdahl, 2006). Our data set consists of arrival times of local earthquakes in the present study region (Figure 2b) and teleseismic events (Figure 2c). The local events were selected based on the following criteria: (1) Each earthquake was recorded at more than four seismic stations in the study region (Figure 2a) and (2) the absolute value of traveltime residuals is smaller than 5.0 s. The teleseismic events located at epicentral distances of 30° to 90° from the center of the study region were selected (Figure 2c), so as to reduce the effects of complex structures near the core-mantle boundary and those in the upper mantle outside the study region (Zhao et al., 1994, 2013). As a result, our data set contains 22,960 arrival times of 2,789 local earthquakes and 4,660 arrival times of 751 teleseismic events, which were recorded at 32 stations in the present study region (Figure 2).

Raw traveltime residuals of the local earthquakes and relative traveltime residuals of the teleseismic events that are within ±2.0 s are simultaneously inverted for a three-dimensional (3-D) velocity model of the crust and upper mantle under the study region using the code TOMOG3D (Zhao et al., 1994, 2012), which is an iterative nonlinear tomographic inversion method. For the teleseismic events, theoretical traveltimes from the hypocenter to the recording stations are first calculated using the one-dimensional (1-D) iasp91 Earth model (Kennett & Engdahl, 1991). Then raw residuals of each teleseismic event are obtained by subtracting the theoretical traveltimes from the observed ones. After removing the mean residual of each teleseismic event from the raw residuals at all the recording stations, relative traveltime residuals of the teleseismic event are obtained. By using the teleseismic relative residuals, the effects of hypocentral mislocations and structural heterogeneities outside the study volume can be greatly reduced (Zhao et al., 1994, 2013).

Figure 3 shows distributions of mean relative traveltime residuals of the teleseismic events at every station. We can see that, in all the four quadrants, early arrivals appear in the eastern and southeastern parts of the Mindanao Island (Figure 3). This result indicates the existence of high-velocity (high-V) anomalies beneath eastern and southeastern Mindanao, in agreement with the distribution of the PT and the Sangihe Trench. In contrast, delayed arrivals mainly exist in the West Mindanao Island (Figure 3), possibly due to the wide distribution of active volcanoes there. Early arrivals are also visible at stations in the

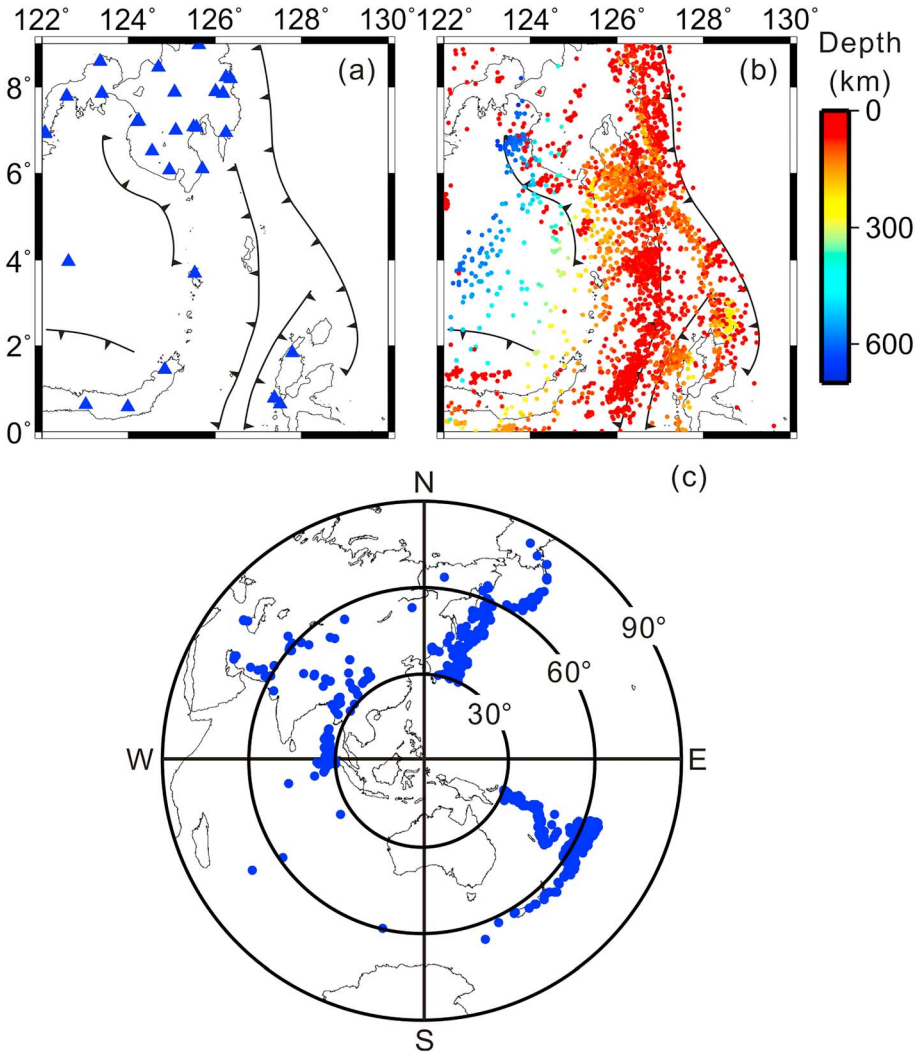

Figure 2. Distribution of (a) seismic stations (blue triangles), (b) local earthquakes (colored dots), and (c) teleseismic events (blue dots), which are used for tomographic inversions in this study. The colors in (b) denote the focal depths. The other symbols are the same as those in Figure 1.

Halmahera Island, especially for the events in the NE and SE quadrants (Figures 3a and 3b), except for the events in the NW quadrant (Figure 3d), which are consistent with the eastward subduction of the Molucca Sea slab along the Halmahera Trench. The distributions of the mean relative residuals at stations in the northeast Sulawesi Island and the Sangihe Arc are different in the four quadrants (Figure 3). Early arrivals dominate in the southern Mindanao Island along the northern end of the Sangihe Trench, whereas delayed arrivals are visible in the Sangihe Arc and the northeastern Sulawesi Island (Figure 3). These remarkable differences of the teleseismic residuals reflect strong lateral heterogeneities in the crust and upper mantle beneath the study region.

To conduct tomographic inversions, we set up a 3-D grid with a horizontal grid interval of 0.5° and a vertical grid interval of 15–100 km (at depths of 5, 20, 50, 100, 150, 200, 250, 300, 400, 500, 600, and 700 km). V_p perturbations at the grid nodes from a 1-D V_p model are taken as unknown parameters. The LSQR algorithm (Paige & Saunders, 1982) with damping and smoothing regularizations is used to solve the system of observation equations that relate the traveltime data to the unknown parameters (Zhao et al., 1994, 2012). The starting 1-D V_p model (Figure 4) is derived from the CRUST1.0 model (Laske et al., 2013) for the crustal velocities and the Moho depth, the WPSP01P model (Wright & Kuo, 2007) for velocities from the Moho to 210-km depth, and the iasp91 Earth model (Kennett & Engdahl, 1991) for

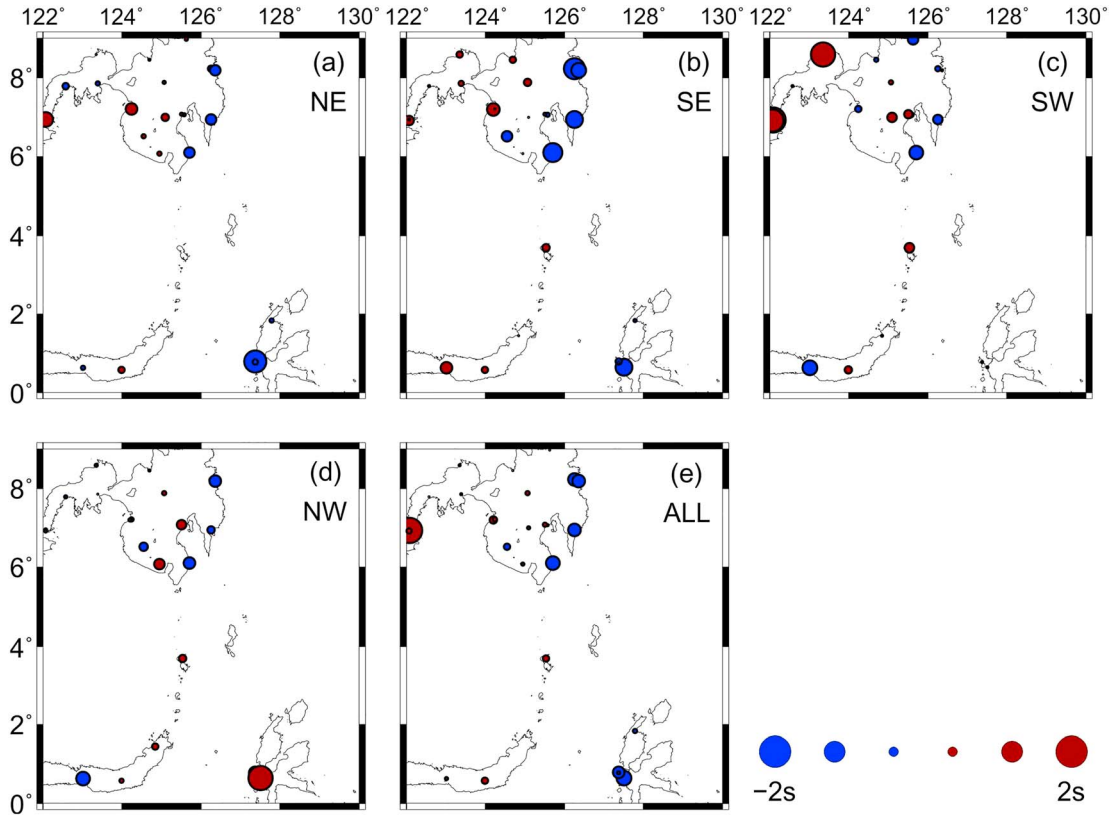

Figure 3. Distributions of mean relative traveltime residuals at every stations from all the teleseismic events (e) and from the events in the (a) NE, (b) SE, (c) SW, and (d) NW quadrants. The blue and red circles denote early and delayed arrivals, respectively, whose scale is shown at the bottom right.

velocities deeper than 210 km. A number of tomographic inversions are conducted (Figures S1–S12 in the supporting information), and the optimal values of the damping and smoothing parameters are found to be 100.0 and 2000.0, respectively (Figure 5), based on the trade-off curve between the root-mean-square traveltime residuals and norms of the obtained 3-D V_p models (Eberhart-Phillips, 1986; Zhao, 2015). For the optimal 3-D V_p model, the root-mean-square traveltime residual is reduced from 1.003 s before the inversion to 0.881 s after a joint inversion of the local and teleseismic data.

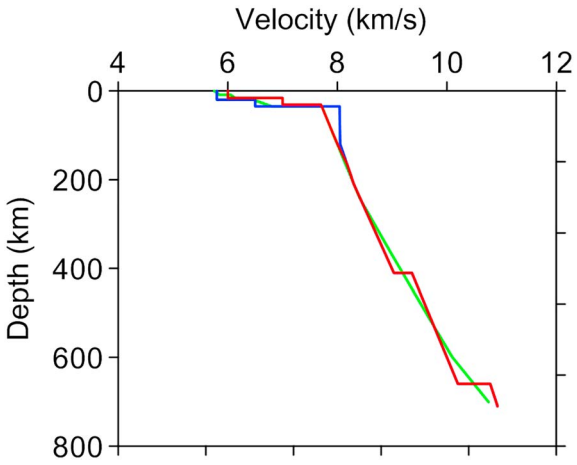

Figure 4. The 1-D starting *P* wave velocity model used in this study (red line), the iasp91 Earth model (blue line; Kennett & Engdahl, 1991), and the WPSP01P model (green line; Wright & Kuo, 2007).

3. Resolution Tests and Tomographic Images

A number of checkerboard resolution tests (CRTs) are conducted to evaluate the resolution of the obtained tomographic images. In the CRT, an initial checkerboard model with V_p perturbations of ±4% at alternate 3-D grid nodes is used to calculate synthetic traveltimes. The numbers and locations of seismic stations, events, and arrival times are the same as those in the observed data set. Random noise with a standard deviation of 0.1 s is added to the synthetic traveltimes to simulate the picking errors in the arrival time data. The synthetic data are then inverted to obtain an output 3-D V_p model. The resolution of the tomographic image can be evaluated by comparing the input checkerboard model with the output V_p model.

Figures 6, 7, and S13 show the results of two CRTs with lateral grid intervals of 0.6° and 1.0°, respectively. The input checkerboard models are well

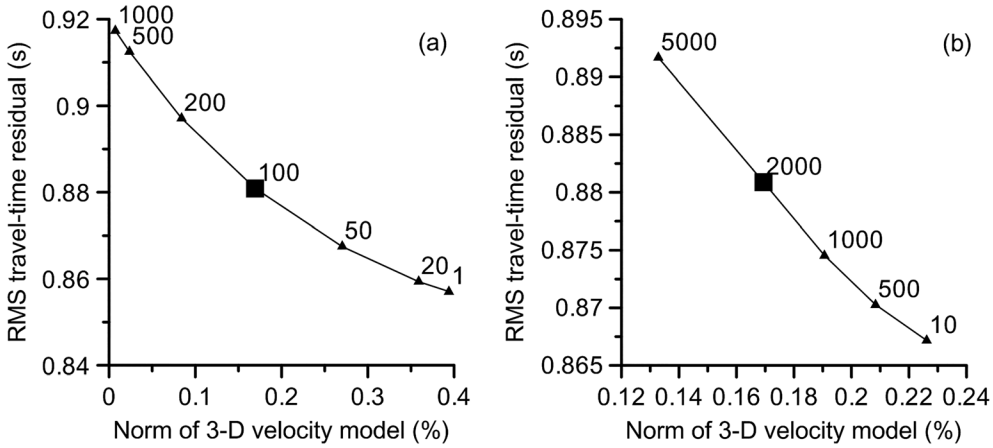

Figure 5. Trade-off curves between the norm of the 3-D velocity model and the root-mean-square (RMS) traveltime residual, with different values (the numbers beside the triangles) of (a) the damping parameter and (b) the smoothing parameter. The squares denote the optimal values of the damping and smoothing parameters.

recovered at most depths of the study region (Figure S14), except for the 5 km depth, where the resolution is good only beneath the Mindanao Island, being consistent with the distribution of ray density (i.e., the number of rays at grid node; Figure 8). The CRT results indicate that our tomographic model has a lateral resolution of 0.6° or better.

Four vertical cross sections and 12 map views at different depths of the obtained V_p tomography are shown in Figures 9 and 10, respectively. Prominent high-V anomalies are revealed, which are inferred to be the subducted Celebes Sea slab along the Cotabato Trench, the Philippine Sea slab along the PT, and the Molucca Sea slab along the Sangihe and Halmahera trenches, respectively, which generally coincide with the Wadati-Benioff deep seismic zones. The Celebes Sea slab is visible down to ~150-km depth along the Cotabato and Sulawesi trenches in cross sections AA′, BB′, and CC′ (Figures 9a–9c), indicating a subduction duration of ~7 Myr assuming a constant convergence rate of ~35 mm/year and a low dip angle of ~35°, which is consistent with the Late Miocene to Pliocene age of the Cotabato Trench (Yumul et al., 2008). The Molucca Sea slab may have subducted down to ~650- and ~150-km depths along the Sangihe and Halmahera trenches, respectively (Figures 9a, 9b, and 9d), in accordance with the previous tomographic results (Hall & Spakman, 2015; Huang et al., 2015). The high-V anomalies associated with the subducted Philippine Sea slab are traceable to depths of 450, 550, and 600 km with an *overturned* dip angle in cross sections AA′, BB′, and CC′, respectively (Figures 9a–9c), being consistent with the tomographic results of Fan et al. (2017). However, the Philippine Sea slab is not visible in cross section DD′ (Figure 9d), probably due to the lower resolution of the tomographic model in that area. The overturned Philippine Sea slab presumably ascribes to the westward subduction of the Molucca Sea slab along the Sangihe Trench. Numerical models (Holt et al., 2017) show that when two plates subduct in the same direction, the mantle dynamic pressure would be elevated due to the subduction of the *front* slab (the Molucca Sea slab) to result in an overturned geometry of the *rear* slab (the Philippine Sea slab), which can explain the morphology of the Philippine Sea slab revealed by our tomography. Low-velocity (low-V) anomalies are revealed above the Molucca Sea slab and parallel with the volcanic front in the Sangihe Arc (Figures 9b–9d and 10a–10c), which may reflect the transition from subduction to collision along the Sangihe and Halmahera trenches (Silver & Moore, 1978).

The reliability of tomographic results can be further confirmed by performing a model-recovery synthetic test (Zhao, 2015; Zhao et al., 1992), which is similar to the CRT, but the input model contains main features of the obtained tomographic image. We performed such synthetic tests (Figures 11 and S15), and the results show that the input anomalies can be recovered very well at all depths beneath the study region (Figures 11 and S15), though slight smearing occurs in some areas because of the imperfect ray coverage and so a lower resolution there. These resolution tests indicate that the main features of our tomographic images are quite robust.

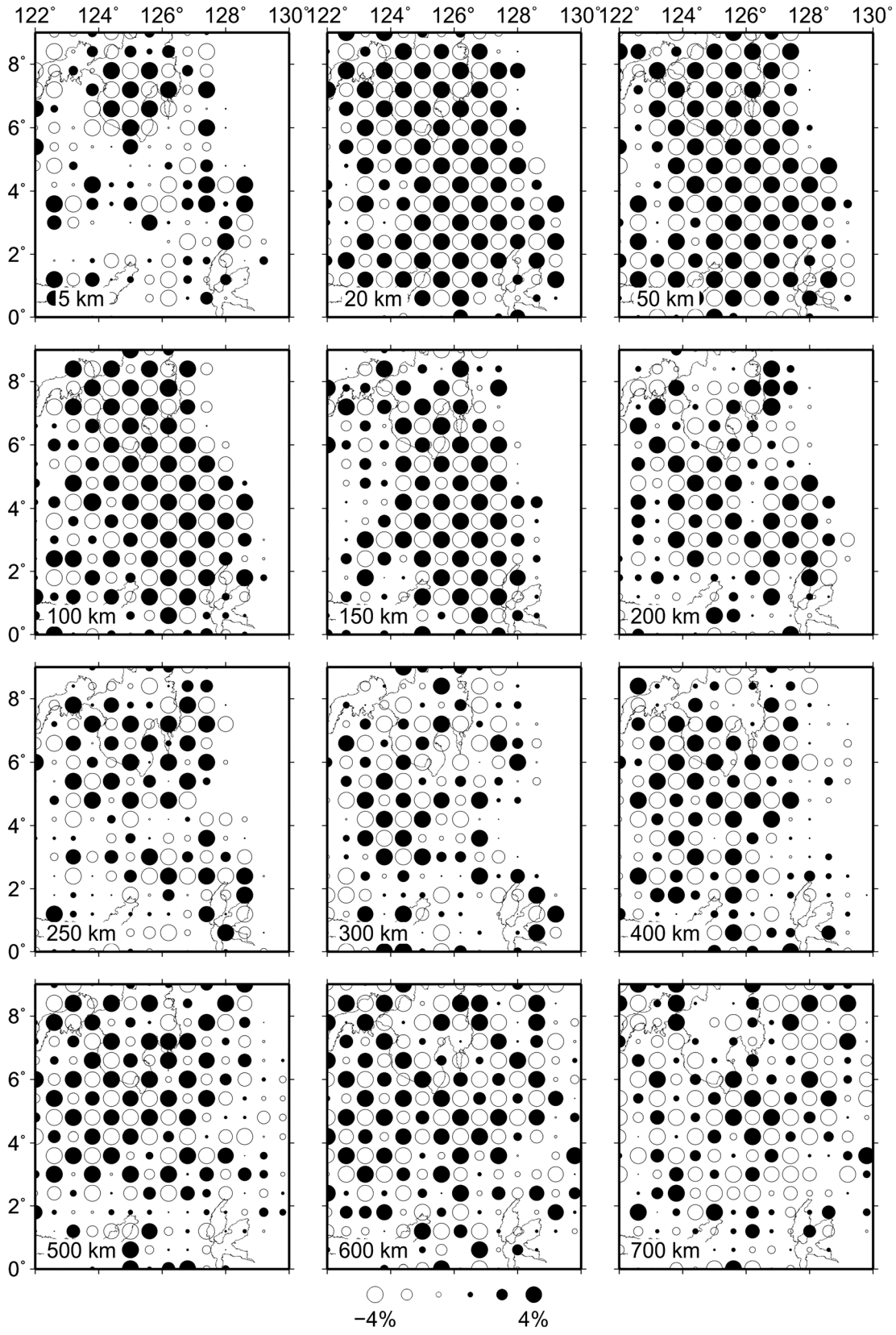

Figure 6. Results of a checkerboard resolution test with a lateral grid interval of 0.6°. The layer depth is shown at the lower left corner of each map. The open and solid circles denote low and high V_P perturbations, respectively, whose scale is shown at the bottom.

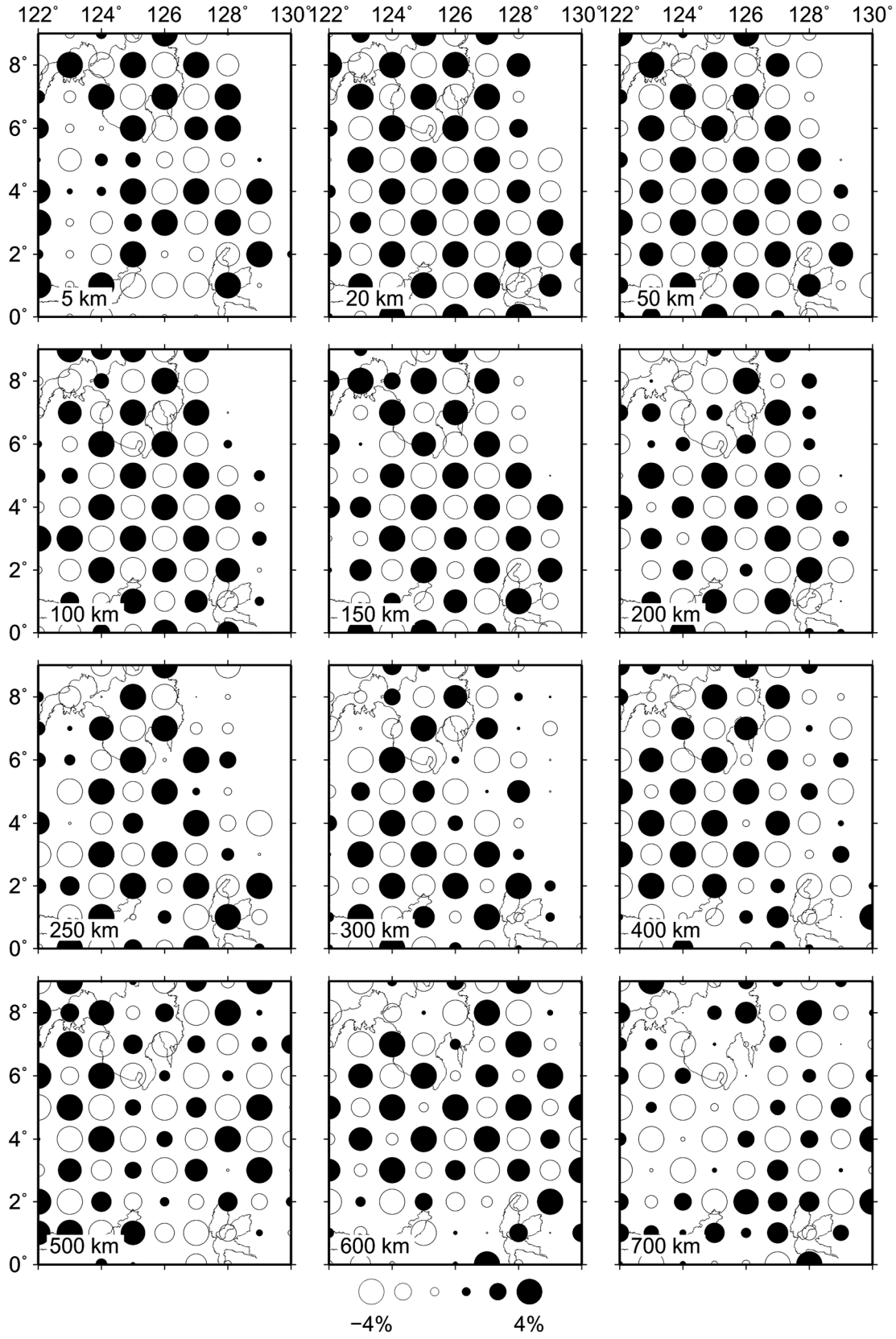

Figure 7. The same as Figure 6 but the lateral grid interval is 1.0°.

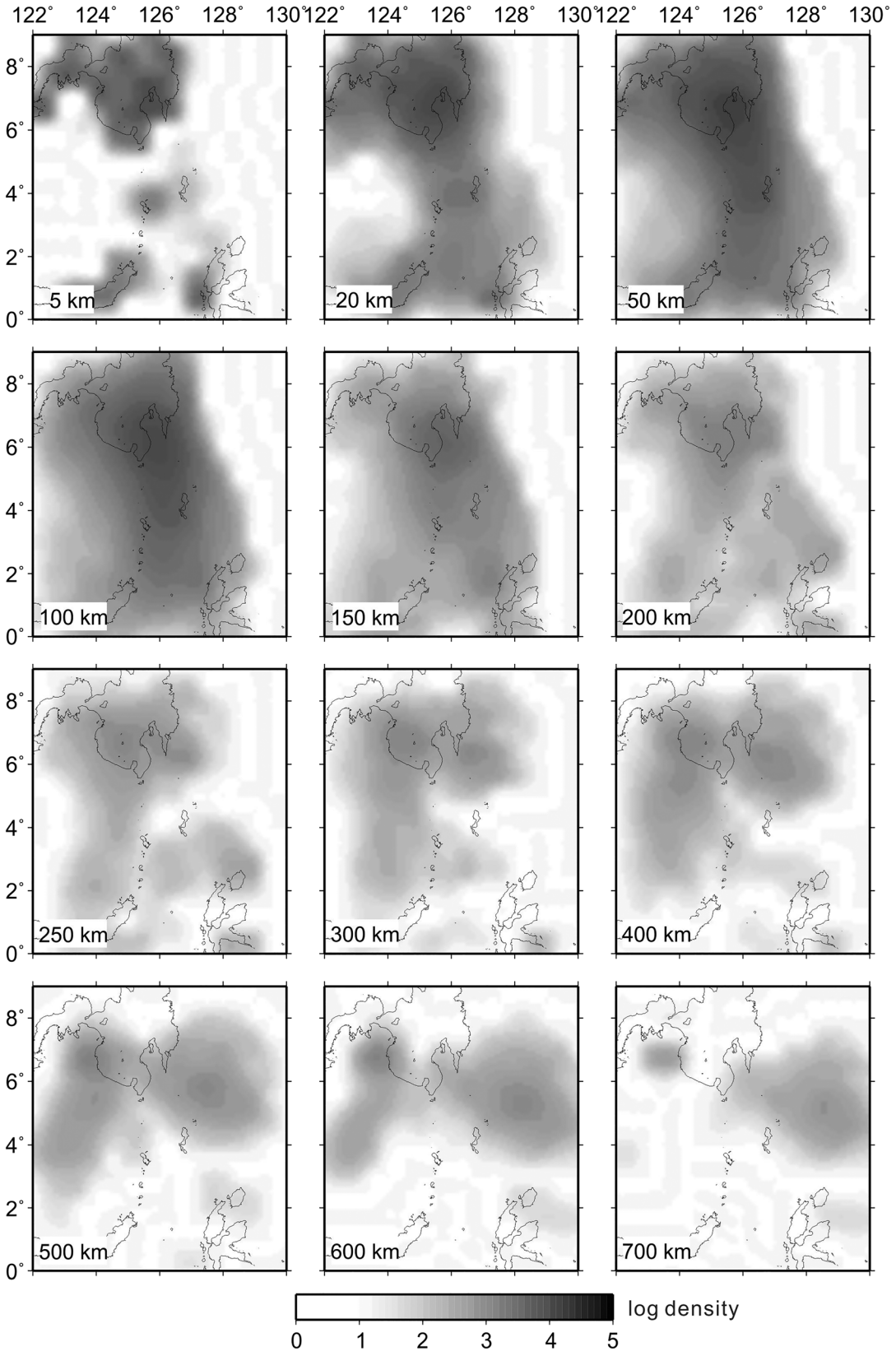

Figure 8. Density distribution of *P* wave rays at different depths. The layer depth is shown at the lower left corner of each map. The ray density scale is shown at the bottom.

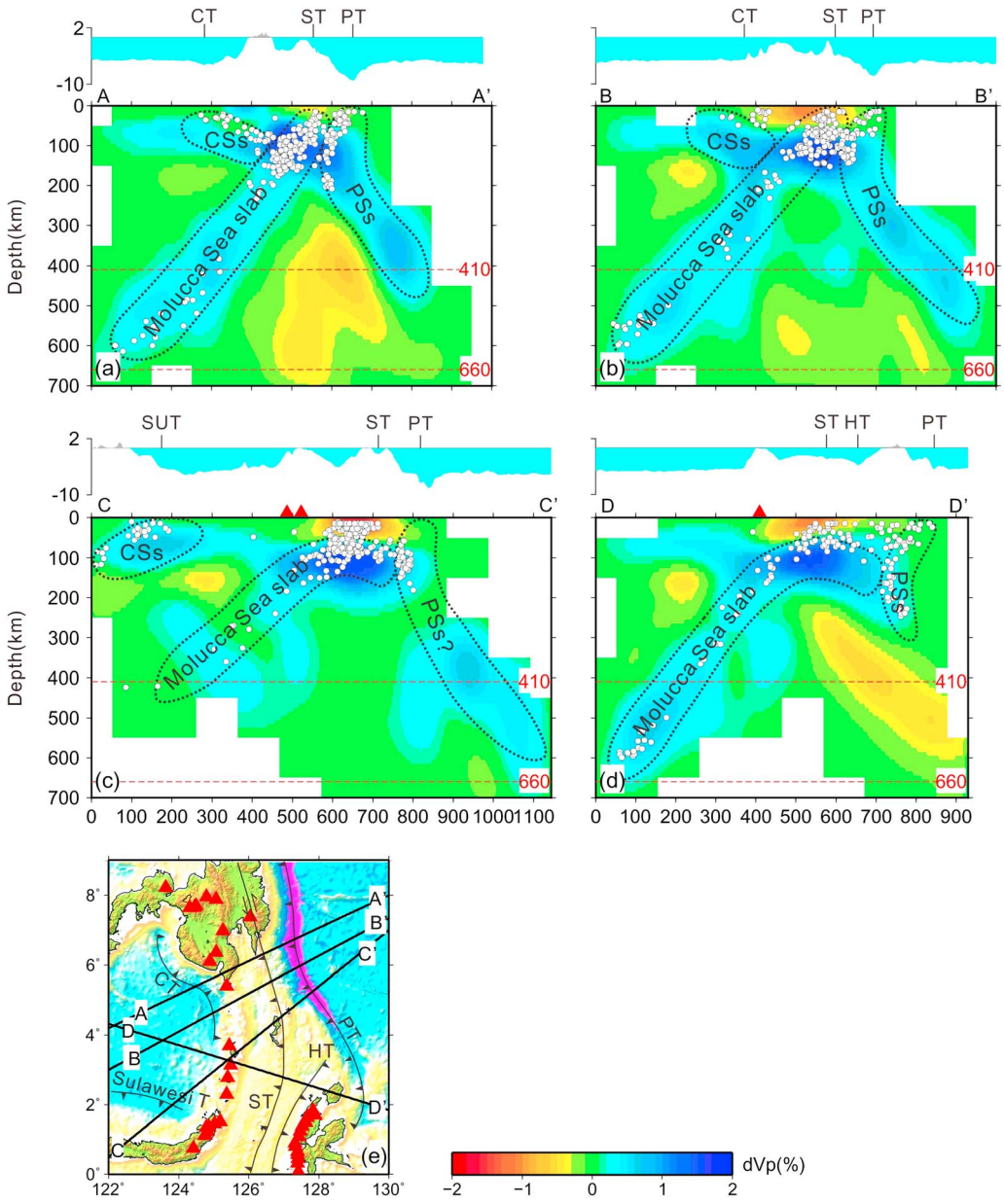

Figure 9. Vertical cross sections of *P* wave tomography obtained with a lateral grid interval of 0.5° along four profiles (a–d) shown in the inset map (e). The surface topography along each profile is shown above the cross sections. The red and blue colors denote low- and high-velocity perturbations, respectively, whose scale is shown at the bottom right. The white dots and red triangles show the background seismicity and active volcanoes, respectively, within a 30-km width of each profile. The black dotted lines show the estimated morphologies of the subducted Celebes Sea slab (CSs), the Molucca Sea slab, and the Philippine Sea slab (PSs). The red horizontal dashed lines denote the 410- and 660-km discontinuities. T = trench; CT = the Cotabato Trench; HT = the Halmahera Trench; PT = the Philippine Trench; ST = the Sangihe Trench; SUT = the Sulawesi Trench. The other symbols are the same as those in Figure 1.

4. Discussion

4.1. Maximum Depths of the Slabs and Comparison With Previous Results

The existence of several trenches and the complexity of earthquake distribution make it difficult to identify the subducted slabs beneath the study region. In our tomographic images (Figures 9 and 10), the subducted Molucca Sea and Celebes Sea slabs along the Sangihe and Cotabato trenches can be identified, but the subducted Molucca Sea and the Philippine Sea slabs along the Halmahera Trench and PT are not very clear.

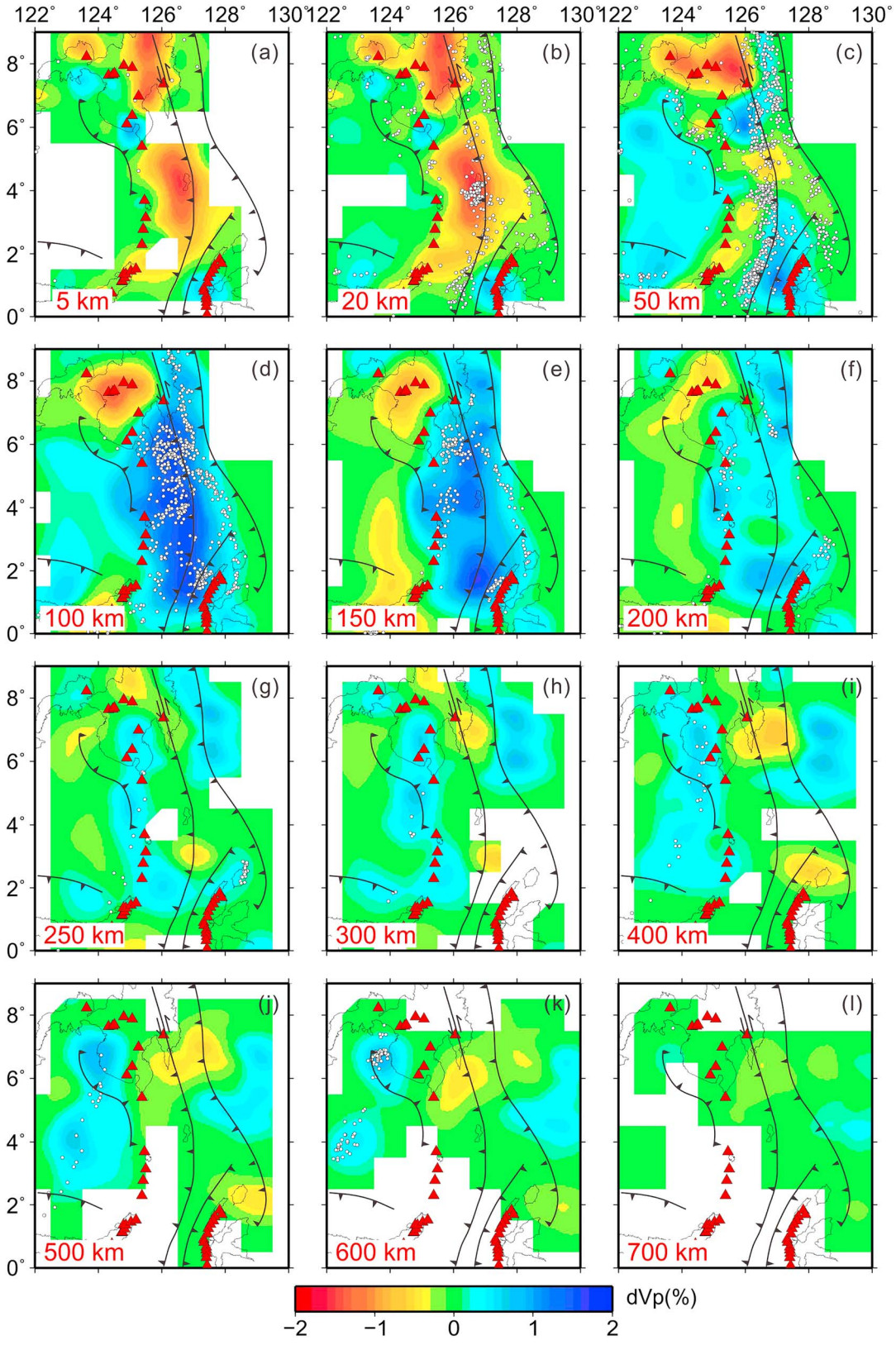

Figure 10. Map views of *P* wave tomography (a–l). The layer depth is shown at the lower left corner of each map. The red triangles denote active volcanoes. The red and blue colors denote low- and high-velocity perturbations, respectively, whose scale is shown at the bottom. The white dots denote seismicity within a depth range of 15–50 km of each layer. The other symbols are the same as those in Figure 1.

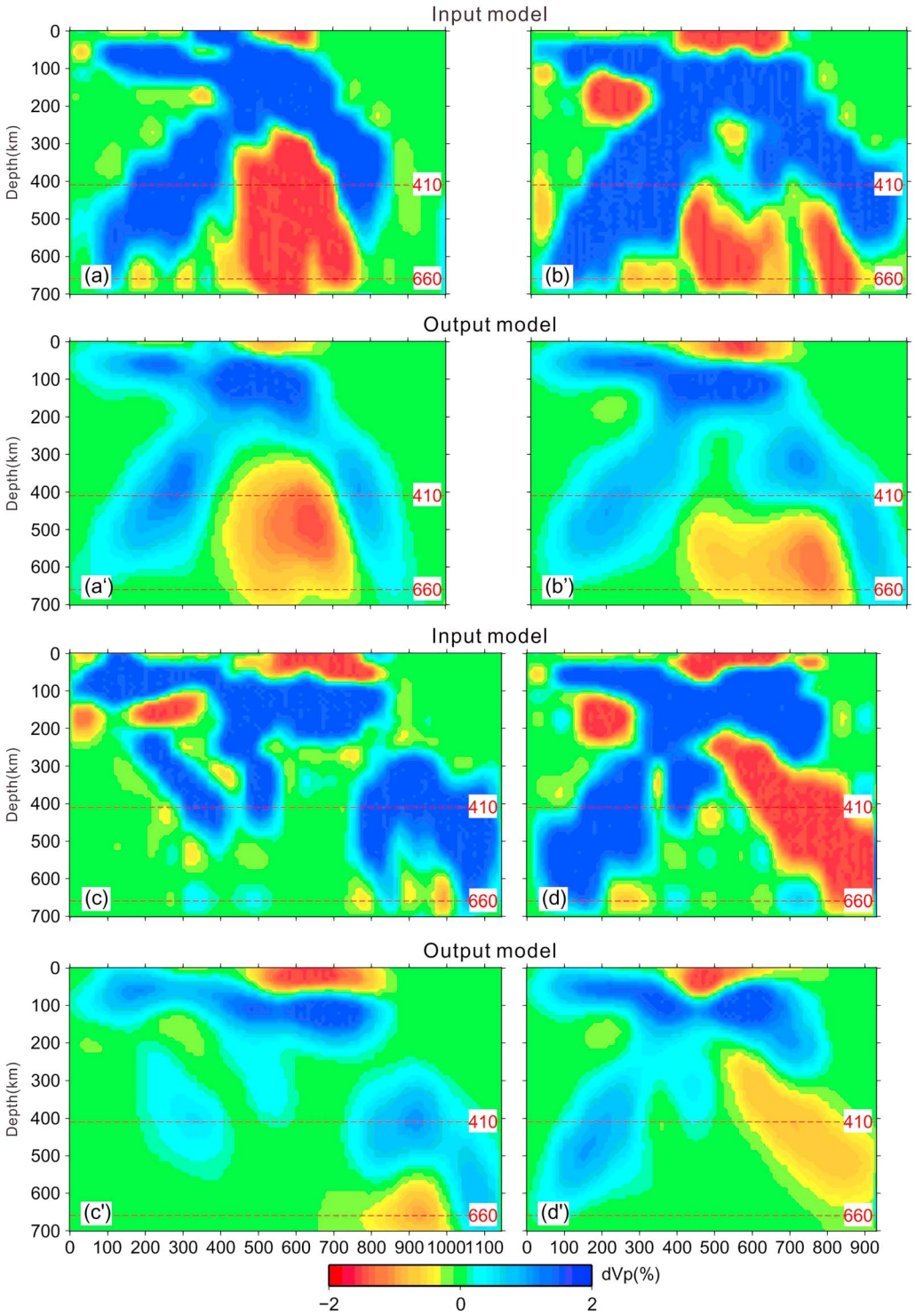

Figure 11. The same as Figure 9 but (a–d) the input model and (a′–d′) output results of a synthetic test (see text for details). The two horizontal dashed lines denote the 410- and 660-km discontinuities. The velocity perturbation scale is shown at the bottom.

Lallemand et al. (1998) suggested that the Snellius Ridge (Figure 1) might represent a remnant of the northern Halmahera Arc that extended to the southeast offshore of the Mindanao Island, indicating that there must be the subducted Molucca Sea slab in the upper mantle north of the current Halmahera

Trench. The high-V anomalies around the 410-km discontinuity in cross sections AA′ to CC′ (Figures 9a–9c) are possible candidates of the slab, which seem not connected with the slab shallower than 200-km depth. This result suggests that the subducted Molucca Sea slab along the Halmahera Trench has detached, which has not been supported by any other results so far. In addition, this feature is not consistent with the trend of the hypocentral distribution. Hence, we think that the high-V anomalies around the 410-km discontinuity in cross sections AA′ to CC′ reflect the subducted Philippine Sea slab along the PT. In cross section DD′ (Figure 9d), the morphology of the subducted Philippine Sea slab is not very clear, because it is located at the edge of our model. Therefore, it is necessary to use a regional or a global tomographic model to know the depth of the subducted Philippine Sea slab along cross section DD′, but such a large-scale tomographic model has a lower resolution.

To data, there have been many studies on the 3-D mantle tomography beneath Southeast Asia in regional (e.g., Hall & Spakman, 2015; Huang et al., 2015) and global scales (e.g., Li et al., 2008; Obayashi et al., 2013; Zhao et al., 2013). Our tomographic images are generally consistent with the previous results, such as the high-V anomalies related to the subducted Malucca Sea slab (Figure S16). However, due to the lower resolution (1.0° or larger) in the crust and uppermost mantle, the slab-related high-V anomalies above ~200-km depth are not revealed by the whole mantle *P* wave tomographic model GAP_P4 (Figure S16), including the subducted Celebes Sea slab along the Sulawesi Trench, where a widespread low-V zone exists. In addition, it is difficult to estimate the morphology of the Philippine Sea slab due to the lower resolution of the GAP_P4 model (Figure S16). Our tomography has a higher resolution enabling to reveal detailed morphologies of the subducted slabs (Figure 9), which shows that the Philippine Sea slab has subducted to depths of 450, 550, and 600 km in cross sections AA′, BB′, and CC, respectively.

The earthquakes in cross section DD′ have a maximum of ~250 km, suggesting that the Philippine Sea slab has subducted to at least that depth. A large low-V anomaly exists beneath the Philippine Sea slab in cross section DD′, which is a reliable features verified by the synthetic tests (Figures 11 and S15). Combining our results (Figure 9) with the global tomography (Figure S16) and the cutoff depths of deep seismicity in all the four cross sections (Figure 9), we deem that the maximum depth of the subducted Philippine Sea slab in cross section DD′ is ~450 km.

4.2. Tectonic Evolution of the Southern PT

Supposing that the convergence rate decreases linearly from ~32 mm/year at ~7°N to ~17 mm/year at ~0°N (Figure 1), the convergence rates at cross sections AA′ to DD′ can be interpolated to be 32.0, 30.9, 29.9, and 21.3 mm/year, respectively. If the convergence rate along the PT southern branch is constant during subduction, it would take 16.8, 20.3, 22.3, and 21.0 Myr for the Philippine Sea slab to reach 450-, 550-, 600-, and 450-km depths, respectively, with overturned near-vertical dip angles in the four cross sections. Sajona et al. (1997) studied geochronology (^{40}K-^{40}Ar dating) of igneous rock samples from the Eastern Mindanao and found that the oldest age of the magmatic rocks is ~18 Myr, suggesting that the initiation time of the subduction beneath the Eastern Mindanao is 20–25 Ma considering the time interval between the subduction initiation and the development of arc volcanoes. According to the plate reconstruction models (e.g., Gaina & Müller, 2007; Hall, 2002), the Eastern Mindanao was located in the south at 20–25 Ma (Figure 12) and has moved northward to its present location since then, suggesting that the oldest magmatism in the Eastern Mindanao was caused by the subduction along the PT southern segment, being consistent with our tomographic results.

Lallemand et al. (1998) estimated that the subduction of the Molucca Sea slab along the Sangihe Trench began at ~30 Ma, whereas Hall and Sparkman (2015) suggested that its initiation time was at ~20 Ma. Despite of the discrepancy between them, it is reasonable to consider the age of the Sangihe Trench to be older than 20 Myr. In addition, Hall (2012) argued that at ~5 Ma, the subduction of the Molucca Sea slab was almost complete and the Halmahera and Sangihe arcs were about to collide, which resulted in the subduction initiation along the PT (Lallemand et al., 1998). However, GPS measurements show that the Molucca Sea collision zone accommodates most of the convergence between the PSP and the Eurasian Plate south of Mindanao, and the rest is mainly absorbed far to the west (Rangin et al., 1999). This result suggests that the Sangihe Trench and the PT southern branch should be contemporaneous rather than a genetic relationship between them, as revealed by our tomography.

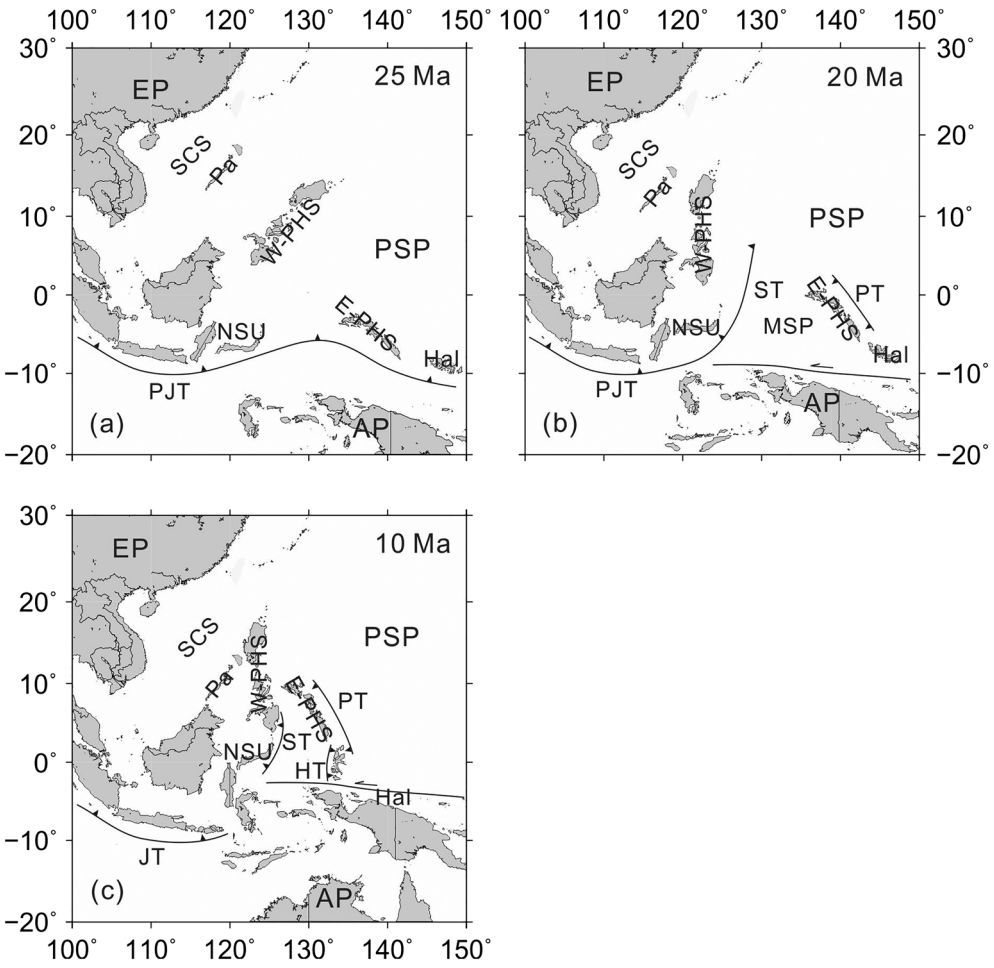

Figure 12. Schematic reconstruction of tectonic evolution around the Philippine Trench (PT) at (a) 25, (b) 20, and (c) 10 Ma. AP = the Australian Plate; EP = the Eurasian Plate; E-PHS = the East Philippines; Hal = the Halmahera Island; HT = the Halmahera Trench; JT = the Java Trench; MSP = the Molucca Sea Plate; NSU = the north Sulawesi Island; Pa = the Palawan block; PJT = the proto Java Trench; PSP = the Philippine Sea Plate; SCS = the South China Sea; ST = the Sangihe Trench; W-PHS = the West Philippines. The other symbols are the same as those in Figure 1.

Although many previous studies have provided significant constraints on the PT origin and tectonic evolution (e.g., Aurelio, 2000; Cardwell et al., 1980; Hall, 1987; Lallemand et al., 1998; Pubellier et al., 1996; Ozawa et al., 2004), they are incongruous with our tomographic results that suggest that the subduction initiation of the PSP along the PT was from the south and not younger than 20–25 Myr. At ~25 Ma (Figure 12a), the Australian Plate subducted beneath the Eurasian and the PSP along the proto Java Trench. During 25–20 Ma (Figure 12b), the Australian Plate started to collide with the Eurasian Plate and the PSP, resulted in the eastern part of the proto Java Trench to be a left-lateral strike-slip fault and the subduction initiation of the Molucca Sea Plate along the Sangihe Trench (Hall, 2002, 2012), as well as the subduction initiation of the PSP beneath the East Philippines along the PT southern segment. The northward movement of the East Philippines (Hall, 2002) engendered the northward propagation of the subduction along the PT. At ~10 Ma (Figure 12c), the Molucca Sea slab subducted to ~660-km depth. The block of the 660-km discontinuity resulted in the subduction termination of the Molucca Sea plate at the Sangihe Trench and its subduction initiation at the Halmahera Trench. The West Philippines began to collide with the Palawan block (e.g., Marchadier & Rangin, 1990) rifted from Mainland Asia (e.g., Holloway, 1982), accompanied with the collision between the West and East Philippines (Hall, 2002). The subduction of the PSP initiated at the central PT and propagated northward (e.g., Fan et al., 2017). Considering the fact that the volcanism in the Philippines near the PT northern

segment started at 6.6 Ma, Ozawa et al. (2004) suggested that the subduction initiated at 8–9 Ma at the northern PT and then propagated southward. However, they overlooked the northward movement of the East Philippines during the last 30 Myr (Hall, 2002). All the volcanic rocks show adakitic characteristics (Ozawa et al., 2004), indicating that the PT northern part has been at the stage of subduction initiation since ~10 Ma, which is reflected in our reconstruction model (Figure 12).

In cross sections AA′–CC′ (Figures 9a–9c), the high-V anomalies associated with the Philippine Sea slab are disconnected at ~200-km depth, being consistent with the maximum focal depths and water depths there but different from those in cross section DD′ (Figure 9d). Assuming a constant convergence rate of ~32 mm/year, it would take ~6.25 Myr for the Philippine Sea slab to reach that depth (~200 km). This may indicate subduction reorganization of the Philippine Sea slab at 6–7 Ma, in agreement with the magmatism gap between 6 and 4.5 Ma (Sajona et al., 1997). At ~5 Ma, the subduction of the Molucca Sea slab was almost complete and the collision between the Sangihe and Halmahera arcs was about to begin (Hall, 2002, 2012), followed by the relative movement variation of the PSP with respect to Eurasia from a northward to a northwestward motion at ~4 Ma (Aurelio, 2000), both of which resulted in the subduction reorganization and initiation of the PSP along the PT southern and northern segments, respectively.

4.3. Tectonic Evolution of the Collision in the Molucca Sea

In our tomographic images, low-V anomalies exist above the subducted Molucca Sea slab in all the four cross sections (Figure 9), which indicate the collision between the West Mindanao-Sangihe Arc and the East Mindanao-Snellius Ridge-Halmahera Arc (Hall, 2002, 2012). It is visible that the low-V anomalies above the subducted Molucca Sea slab in cross section AA′ (Figure 9a) are less significant than those in cross sections BB′–DD′ (Figures 9b–9d), implying that the completion of the Molucca Sea subduction along the Sangihe Trench propagated from the south to the north. This feature is also consistent with the distribution of deep earthquakes whose distance from the Sangihe Trench to the south is larger than that to the north at depths of 200–600 km (Figures 10f–10k), suggesting that the Molucca Sea slab is steeper in the north than in the south, further indicating that the Molucca Sea slab in the south has sunk into the deeper upper mantle. Therefore, the termination of the Molucca Sea slab subduction along the Sangihe Trench may be earlier than 5 Ma.

4.4. Origin of the Central and Southern PF

At depths of 400–600 km (Figures 9i–9k), similar to the deep seismicity, the high-V anomalies associated with the subducted Molucca Sea slab are far north of the northern end of the Sangihe Trench at the same latitude of the southern segment of the PF. Both of the features suggest that the central and southern segments of the PF possibly originated from the subduction termination of the Molucca Sea slab along the Sangihe Trench at ~5 Ma (Aurelio, 2000), coinciding with the discontinuity of the low-V anomalies at 20-km depth (Figure 10b) and the abrupt change of low-V to high-V anomalies at 50-km depth (Figure 10c) beneath the PF and the Sangihe Trench.

5. Conclusions

In this work we investigate the detailed 3-D *P* wave velocity structure of the crust and upper mantle beneath the PT southern branch. Our results provide new constraints on the PT tectonic evolution and the subduction termination of the Molucca Sea slab along the Sangihe Trench. The subducted Philippine Sea slab is visible down to 450- to 600-km depths with an overturned dip angle along the PT southern segment. Assuming a constant convergence rate along the PT southern branch, it would take ~15 to ~23 Myr for the Philippine Sea slab to reach 450- to 600-km depths. Combining our tomographic results with geochronology of the igneous rocks from the Eastern Mindanao with the oldest age of ~18 Myr, we think that the subduction along the southern segment of the PT possibly initiated at 20–25 Ma, which indicates contemporaneity between the PT and the Sangihe Trench. At ~10 Ma, the collision among the West Philippines, the Palawan block, and the East Philippines induced the subduction initiation of the PSP at the central PT and propagated northward. The subduction of the Molucca Sea slab along the Sangihe Trench possibly completed progressively northward from ~5 Ma, which may be the cause of the subduction reorganization and initiation of the PSP along the PT southern and northern segments, respectively.

Acknowledgments

We are very grateful to Prof. Maureen Long (the Editor) and two anonymous reviewers who provided constructive comments and suggestions that have improved this paper. The *P* wave arrival time data used in this study are accessed at the ISC database: http://www.isc.ac.uk/isc-ehb/. This work was financially supported by the National Natural Science Foundation of China (grant 41506059) and the National Special Project for Global Change and Air-Sea Interaction (GASI-GEOGE-02) to J. Fan, as well as research grants from Japan Society for the Promotion of Science (Kiban-S 23224012) and Ministry of Education, Culture, Sports, Science and Technology (MEXT; Shin-Gakujutsu 26106005) to D. Zhao. Most of the figures are made using the GMT software package (Wessel & Smith, 1998).

References

Aurelio, M. A. (2000). Shear partitioning in the Philippines: Constraints from Philippine Fault and global positioning system data. *Island Arc*, *9*(4), 584–597. https://doi.org/10.1046/j.1440-1738.2000.00304.x

Cardwell, R. K., Isacks, B. L., & Karig, D. E. (1980). The spatial distribution of earthquakes, focal mechanism solutions, and subducted lithosphere in the Philippine and northern Indonesian islands. *American Geophysical Union Monograph*, *23*, 1–35.

Eberhart-Phillips, D. (1986). Three-dimensional velocity structure in northern California Coast Ranges from inversion of local earthquake arrival times. *Bulletin of the Seismological Society of America*, *76*, 1025–1052.

Engdahl, E. R. (2006). Application of an improved algorithm to high precision relocation of ISC test events. *Physics of the Earth and Planetary Interiors*, *158*(1), 14–18. https://doi.org/10.1016/j.pepi.2006.03.007

Engdahl, E. R., van der Hilst, R., & Buland, R. (1998). Global teleseismic earthquake relocation with improved travel times and procedures for depth determination. *Bulletin of the Seismological Society of America*, *88*, 722–743.

Fan, J., Zhao, D., Dong, D., & Zhang, G. (2017). *P*-wave tomography of subduction zones around the central Philippines and its geodynamic implications. *Journal of Asian Earth Sciences*, *146*, 76–89. https://doi.org/10.1016/j.jseaes.2017.05.015

Gaina, C., & Müller, D. (2007). Cenozoic tectonic and depth/age evolution of the Indonesian gateway and associated back-arc basins. *Earth-Science Reviews*, *83*(3-4), 177–203. https://doi.org/10.1016/j.earscirev.2007.04.004

Global Volcanism Program, 2013. Volcanoes of the world, v. 4.6.7. Venzke, E (ed.). Smithsonian Institution. Downloaded 02 Apr 2018. https://doi.org/10.5479/si.GVP.VOTW4-2013

Hall, R. (1987). Plate boundary evolution in the Halmahera region, Indonesia. *Tectonophysics*, *144*(4), 337–352. https://doi.org/10.1016/0040-1951(87)90301-5

Hall, R. (2002). Cenozoic geological and plate tectonic evolution of SE Asia and the SW Pacific: Computer-based reconstructions, model and animations. *Journal of Asian Earth Sciences*, *20*(4), 353–431. https://doi.org/10.1016/S1367-9120(01)00069-4

Hall, R. (2012). Late Jurassic–Cenozoic reconstructions of the Indonesian region and the Indian Ocean. *Tectonophysics*, *570-571*, 1–41. https://doi.org/10.1016/j.tecto.2012.04.021

Hall, R., & Spakman, W. (2015). Mantle structure and tectonic history of SE Asia. *Tectonophysics*, *658*, 14–45. https://doi.org/10.1016/j.tecto.2015.07.003

Holloway, N. H. (1982). North Palawan block, Philippines: Its relation to Asian mainland and role in evolution of South China Sea. *American Association of Petroleum Geologists Bulletin*, *16*, 1355–1383.

Holt, A. F., Royden, L. H., & Becker, T. W. (2017). The dynamics of double slab subduction. *Geophysical Journal International*, *209*, 250–265.

Huang, Z., Zhao, D., & Wang, L. (2015). *P* wave tomography and anisotropy beneath Southeast Asia: Insight into mantle dynamics. *Journal of Geophysical Research: Solid Earth*, *120*, 5154–5174. https://doi.org/10.1002/2015JB012098

Kennett, B. L. N., & Engdahl, E. R. (1991). Traveltimes for global earthquake location and phase identification. *Geophysical Journal International*, *105*(2), 429–465. https://doi.org/10.1111/j.1365-246X.1991.tb06724.x

Lallemand, S. E., Popoff, M., Cadet, J. P., Bader, A. G., Pubellier, M., Rangin, C., & Deffontaines, B. (1998). Genetic relations between the central and southern Philippine trench and the Sangihe trench. *Journal of Geophysical Research*, *103*, 933–950. https://doi.org/10.1029/97JB02620

Laske, G., Masters, G., Ma, Z., & Pasyanos, M. (2013). Update on CRUST1.0 - A 1-degree global model of Earth's CRUST. Geophysical Research Abstracts, 15, Abstract EGU, 2013–2658.

Li, C., van der Hilst, R. D., Engdahl, E. R., & Burdick, S. (2008). A new global model for *P* wave speed variations in Earth's mantle. *Geochemistry, Geophysics, Geosystems*, *9*, Q05018. https://doi.org/10.1029/2007GC001806

Marchadier, Y., & Rangin, C. (1990). Polyphase tectonics at the southern tip of the Manila trench, Mindoro-Tablas islands, Philippines. *Tectonophysics*, *183*(1-4), 273–287. https://doi.org/10.1016/0040-1951(90)90421-4

Obayashi, M., Yoshimitsu, J., Nolet, G., Fukao, Y., Shiobara, H., Sugioka, H., et al. (2013). Finite frequency whole mantle *P* wave tomography: Improvement of subducted slab images. *Geophysical Research Letters*, *40*, 5652–5657. https://doi.org/10.1002/2013GL057401

Ozawa, A., Tagami, T., Listanco, E. L., Arpa, C. B., & Sudo, M. (2004). Initiation and propagation of subduction along the Philippine Trench: Evidence from the temporal and spatial distribution of volcanoes. *Journal of Asian Earth Sciences*, *23*(1), 105–111. https://doi.org/10.1016/S1367-9120(03)00112-3

Paige, C. C., & Saunders, M. A. (1982). LSQR: An algorithm for sparse linear equations and sparse least squares. *ACM Transactions on Mathematical Software*, *8*(1), 43–71. https://doi.org/10.1145/355984.355989

Pubellier, M., Quebral, R., Aurelio, M., & Rangin, C. (1996). Docking and post-docking escape tectonics in the southern Philippines. *Geological Society, London, Special Publications*, *106*(1), 511–523. https://doi.org/10.1144/GSL.SP.1996.106.01.32

Rangin, C., Le Pichon, X., Mazzotti, S., Pubellier, M., Chamot-Rooke, N., Aurelio, M., et al. (1999). Plate convergence measured by GPS across the Sundaland/Philippine Sea plate deformed boundary: The Philippines and eastern Indonesia. *Geophysical Journal International*, *139*(2), 296–316. https://doi.org/10.1046/j.1365-246x.1999.00969.x

Sajona, F. G., Bellon, H., Maury, R. C., Pubellier, M., Quebral, R. D., Joseph, C., et al. (1997). Tertiary and Quaternary magmatism in Mindanao and Leyte (Philippines): Geochronology, geochemistry and tectonic setting. *Journal of Asian Earth Sciences*, *15*, 121–153.

Silver, E. A., & Moore, J. C. (1978). The Molucca collision zone, Indonesia. *Journal of Geophysical Research*, *83*, 1681–1691. https://doi.org/10.1029/JB083iB04p01681

Smith, W. H. F., & Sandwell, D. T. (1997). Global seafloor topography from satellite altimetry and ship depth soundings. *Science*, *277*, 1957–1962.

Wessel, P., & Smith, W. (1998). New, improved version of generic mapping tools released. *Eos, Transactions American Geophysical Union*, *79*(47), 579. https://doi.org/10.1029/98EO00426

Wright, C., & Kuo, B. (2007). Evidence for an elevated 410 km discontinuity below the Luzon, Philippines region and transition zone properties using seismic stations in Taiwan and earthquake sources to the south. *Earth, Planets and Space*, *59*(6), 523–539. https://doi.org/10.1186/BF03352715

Yumul, G. P., Dimalanta, C. B., Maglambayan, V., & Marquez, E. J. (2008). Tectonic setting of a composite terrane: A review of the Philippine island arc system. *Geosciences Journal*, *12*(1), 7–17. https://doi.org/10.1007/s12303-008-0002-0

Zhao, D. (2015). *Multiscale seismic tomography* (p. 304). New York: Springer. https://doi.org/10.1007/978-4-431-55360-1

Zhao, D., Hasegawa, A., & Horiuchi, S. (1992). Tomographic imaging of P and S wave velocity structure beneath northeastern Japan. *Journal of Geophysical Research*, *97*, 19,909–19,928.

Zhao, D., Hasegawa, A., & Kanamori, H. (1994). Deep structure of Japan subduction zone as derived from local, regional, and teleseismic events. *Journal of Geophysical Research*, *99*, 22,313–22,329. https://doi.org/10.1029/94JB01149

Zhao, D., Yamamoto, Y., & Yanada, T. (2013). Global mantle heterogeneity and its influence on teleseismic regional tomography. *Gondwana Research*, *23*(2), 595–616. https://doi.org/10.1016/j.gr.2012.08.004

Zhao, D., Yanada, T., Hasegawa, A., Umino, N., & Wei, W. (2012). Imaging the subducting slabs and mantle upwelling under the Japan Islands. *Geophysical Journal International*, *190*(2), 816–828. https://doi.org/10.1111/j.1365-246X.2012.05550.x